JOURNAL OF CATALYSIS **175,** 220–225 (1998)
ARTICLE NO. CA982016

Enhanced Catalytic Activity of Air-Calcined Fluorination Catalyst

Young Su Chung,* Hyunjoo Lee,† Hyun Dam Jeong,*,[1] Yu Kwon Kim,* Han Gil Lee,*
Hoon Sik Kim,† and Sehun Kim*,[2]

*Center for Molecular Science and Department of Chemistry, Korea Advanced Institute of Science and Technology, Taejon 305-701, Korea; and †Korea Institute of Science and Technology, P.O. Box 131, Cheongrayng, Seoul 130-650, Korea

Received August 4, 1997; revised November 25, 1997; accepted January 12, 1998

The catalytic activity of the air-calcined catalyst of $CrF_3 \cdot 4H_2O$ for the fluorination reaction of CF_3CH_2Cl was found to be 20 times higher than that of $CrF_3 \cdot 4H_2O$. Photoacoustic spectroscopy measurements and XPS revealed the existence of various chromium phases and an increased density-of-states near the Fermi energy level in this catalyst. The increased catalytic activity of the air-calcined sample is attributed to the relatively easier formation of labile fluorine on the catalyst surface due to the stronger interaction between the valence band of CrO_xF_y and the antibonding orbitals of HF.

I. INTRODUCTION

CF_3CH_2F (HFC-134a) has been considered as one of the most promising candidates for the substitution of CFC-12 (CF_2Cl_2) (1–8). One of the synthetic routes to HFC-134a is the vapor-phase fluorination of CF_3CH_2Cl (HCFC-133a) with HF over Cr- or Al-based catalysts (9–14). Among various fluorination catalysts, $CrF_3 \cdot 4H_2O$ was expected to be the first candidate catalyst on the assumption that the high fluorine-containing catalyst might have a better catalytic activity and a longer lifetime (15, 16). Contrary to our expectation, the fluorination of HFC-133a with HF over $CrF_3 \cdot 4H_2O$ gave only a small amount of the desired product, HFC-134a, and an appreciable amount of unwanted product, $CF_2{=}CHCl$ (HCFC-112), under a typical reaction condition. Another candidate catalyst was prepared through air-calcination of $CrF_3 \cdot 4H_2O$. The catalytic activity of this air-calcined catalyst for the above fluorination reaction was 20 times higher than that of the $CrF_3 \cdot 4H_2O$ catalyst. A similar result was obtained for the fluorination of CF_3CHCl_2 to CF_3CHF_2 (HFC-125), a substitute for $CF_2HCl + CF_3CF_2Cl$ (R-502). The air-calcination gives rise to the loss of water and a hydrolysis reaction in which the water molecules hydrolyze the Cr–F bonds, thus creating Cr–O bonds. The chemical composition of the air-calcined product is therefore assumed to be CrO_xF_y. In order to elucidate the enhanced catalytic activity of the air-calcined catalyst, we have in this work investigated the changes of the structural and electronic properties of the chromium fluoride catalyst due to air-calcination, using X-ray diffraction (XRD), X-ray photoelectron spectroscopy (XPS), photoacoustic spectroscopy (PAS).

II. EXPERIMENTAL

$CrF_3 \cdot 4H_2O$ was commercially purchased from Aldrich company. The CrO_xF_y catalyst examined in this study was prepared by air-calcination of $CrF_3 \cdot 4H_2O$ at 673 K for 5 h. The fluorination reactions were performed in a fixed-bed reactor made of Inconel 600 tubing, with 1 in. diameter and 30 cm long, equipped with an electrical heater. Thirty grams of pelleted catalyst was loaded into the reactor and dried *in situ* at 673 K for 1 h in He at a flow of 200 ml/min. The activation process was followed with 400 ml/min HF at 473 K for 2 h and subsequently at 673 K. Flow rates of CF_3CH_2Cl, HF and CF_3CHCl_2 preheated in a chamber at 318 K were carefully controlled using Matheson mass flow controllers. The effluent reaction mixture was analyzed by on-line Gaw-Mac 580P TCD GC equipped with a 6-f porapak N column after being scrubbed with H_2O and dried over molecular sieve 4A.

The crystalline structures of the two catalyst samples were investigated by XRD using Cu-Kα radiation (30 kV, 40 mA) with a Ni filter. The crystalline phases were identified by the comparison of measured XRD patterns of the catalysts with JCPDS powder diffraction file data.

The XPS measurements were conducted with a VG Scientific ESCALAB 220 spectrometer, equipped with a hemispherical energy analyzer. The nonmonochromatized Al-Kα X-ray source ($h\nu = 1486.6$ eV) was operated at 12.5 kV and 16 mA. Before data-acquisition, the pellet type samples were outgassed for about 3 h at 373 K under a pressure of $\sim 1.0 \times 10^{-2}$ Torr to minimize the surface contamination. The obtained XPS spectra were fitted using a nonlinear least square method.

[1] Present address: Semiconductor R&D center, Samsung Electronics Co., LTD., Yongin-City, Kyungki-Do, 449-900, Korea.
[2] Corresponding author.

0021-9517/98 $25.00

The PAS spectra were obtained with a homemade photoacoustic spectrometer. A 1-kW high-pressure Xe lamp (Oriel model 6269) was used as a light source, modulated by a mechanical chopper. The PA signal, detected by an electric microphone, was amplified by a preamplifier (SRS model 550) and a lock-in amplifier (SRS model 530).

The conductivity measurements were performed by measuring the current under constant voltage with a surface conductivity type cell on an area of 12×10 mm^2 with a picoammeter (Keithley 485).

III. RESULTS AND DISCUSSION

The fluorination reactions of CF_3CH_2Cl, and CF_3CHCl_2 were studied in a fixed bed reactor:

$$CF_3CH_2Cl + HF \rightarrow CF_3CH_2F \quad [1]$$

$$CF_3CHCl_2 + HF \rightarrow CF_3CHClF + CF_3CHF_2 \quad [2]$$

Figure 1 shows that the air-calcined CrO_xF_y catalyst exhibits a much higher catalytic activity than $CrF_3 \cdot 4H_2O$. The XRD pattern of the newly formed species is quite different from that of $CrF_3 \cdot 4H_2O$, as shown in Fig. 2, which indicates the presence of new crystalline phases after air-calcination. The XRD pattern of this CrO_xF_y material does not match with any of the chromium species listed in the JCPDS handbook. The crystalline phase in the CrO_xF_y sample is not identified yet. However, the much weaker diffraction peak intensity of the CrO_xF_y relative to $CrF_3 \cdot 4H_2O$ indicates

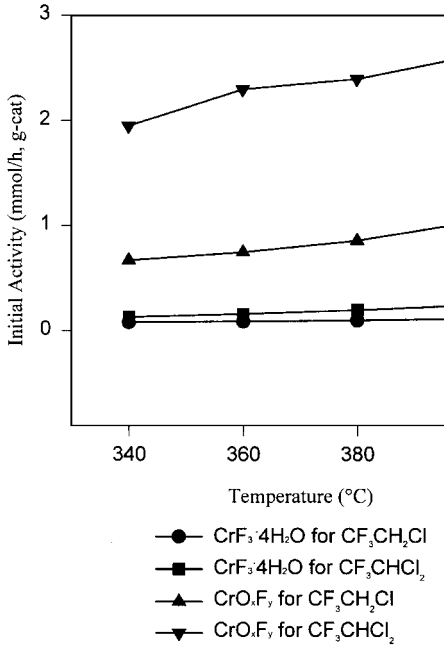

FIG. 1. Catalytic activities of $CrF_3 \cdot 4H_2O$ and CrO_xF_y as a function of reaction temperature in the fluorination of CF_3CH_2Cl and CF_3CHCl_2.

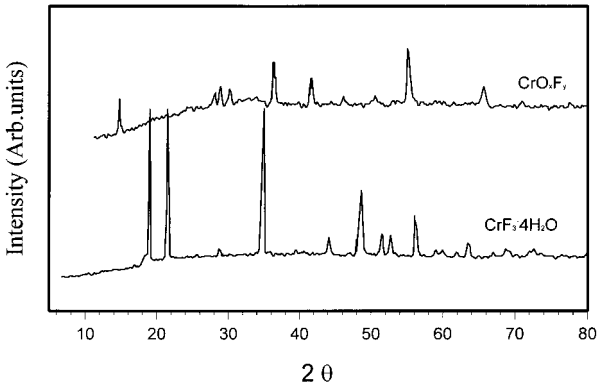

FIG. 2. XRD patterns of $CrF_3 \cdot 4H_2O$ and CrO_xF_y.

that the CrO_xF_y catalyst contains predominantly noncrystalline phases.

X-ray photoelectron spectroscopy (XPS) was applied to identify the chemical states of the $CrF_3 \cdot 4H_2O$ and CrO_xF_y samples. The high resolution Cr 2p core level spectra of these samples are shown in Fig. 3a. The Cr $2p_{3/2}$ core level spectrum of $CrF_3 \cdot 4H_2O$ shows a single peak at 579.7 eV which is consistent with previous measurements for $CrF_3 \cdot 4H_2O$ (17–19). On the other hand, the spectrum of CrO_xF_y shows three curve-fitted peaks at 576.7, 579.7, and 581.7 eV, indicating the existence of various chromium species. The peak at 579.7 eV is ascribed to the CrF_3 phase. In addition, the peak at 576.7 eV is tentatively assigned to the amorphous Cr_2O_3 phase (19), although its crystalline phase is not observed in the XRD measurement. Finally, the weak peak at 581.7 eV is likely due to chromium species with higher oxidation states than Cr^{+3}. Blanchard *et al.* showed that in a set of temperature-programmed oxidation and reduction experiments, the fluorination activity of chromia is greatly influenced by the presence of chromium in higher oxidation state (20). Kemnitz *et al.* also reported the existence of chromium in higher oxidation states (21). In fact, the measurement of the high valent ($>+3$) chromium by the titration technique (4, 22) showed that CrO_xF_y has an appreciable oxidizing capacity, ca 5.3×10^{-3} F/g catalyst, unlike $CrF_3 \cdot 4H_2O$, whose oxidizing capacity is negligible. We also note the broad feature of the chromium peak after air-calcination. This implies the existence of nonstoichiometric, disordered chromium species through air-calcination.

The high-resolution F 1s core level spectra in Fig. 3b show two peaks at 685.3 and 687.7 eV for the CrO_xF_y sample and a single peak at 685.6 eV for $CrF_3 \cdot 4H_2O$. The relatively weaker peak at 685.3 eV in CrO_xF_y indicates the presence of CrF_3. The peak at 687.7 eV is ascribed to a new chromium fluoride phase CrO_xF_y.

The high-resolution O 1s core level spectra of the catalysts are shown in Fig. 3c. The O 1s spectrum of $CrF_3 \cdot 4H_2O$ shows a prominent peak at 532.5 eV due to the oxygen

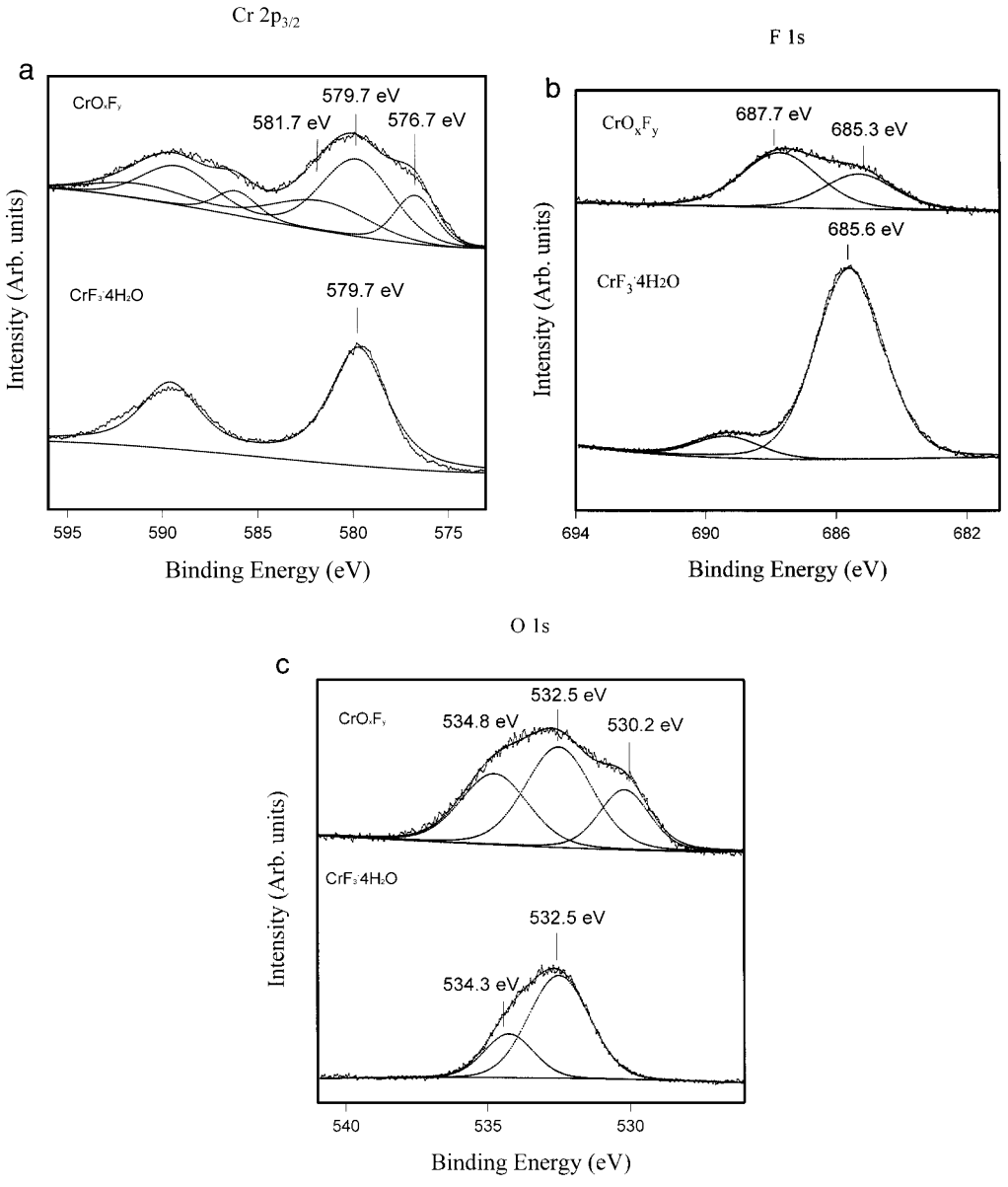

FIG. 3. XPS core level spectra of (a) Cr $2p_{3/2}$, (b) F 1s, (c) O 1s for $CrF_3 \cdot 4H_2O$ and CrO_xF_y.

atoms of intrinsic water molecules and a peak at 534.3 eV assigned to surface hydroxyl groups. The O 1s spectrum of the CrO_xF_y sample shows three peaks of 530.2, 532.5, and 534.8 eV. The peak at 532.5 eV is ascribed in part to the remaining water molecule and in part to CrO_xF_y, while the peak at 534.8 eV is assigned to the oxygen atoms of surface hydroxyl groups. In addition, the peak at 530.2 eV is assigned to the oxygen atom of Cr_2O_3.

The PAS spectra for $CrF_3 \cdot 4H_2O$ and CrO_xF_y are shown in Fig. 4. The $CrF_3 \cdot 4H_2O$ sample shows two bands at ca 400 and ca 600 nm, which are assigned to the $^4T_{1g} \leftarrow {}^4A_{2g}$ and $^4T_{2g} \leftarrow {}^4A_{2g}$ d-d transitions, respectively, in a transition metal complex of octahedral geometry (23). The energy of the first spin-allowed transition $^4T_{1g} \leftarrow {}^4A_{2g}$ directly gives the value of the ligand field splitting, 10 Dq. The value of 10 Dq for $CrF_3 \cdot 4H_2O$ is estimated to be ca 16700 cm^{-1}, which is higher than that of $[CrF_6]^{3-}$ (15200 cm^{-1}), but lower than that of $[Cr(H_2O)_6]^{3+}$ (17400 cm^{-1}) (24). This indicates that both F^- and H_2O ligands are directly coordinated to the chromium ions in $CrF_3 \cdot 4H_2O$ sustaining the octahedral geometry. In the CrO_xF_y sample, however, no noticeable peak is observed in the range of 300 to 700 nm. A flat PAS signal can mean that the sample contains a mixture of several Cr^{+3} species. This observation is also in good agreement with the XPS result that the CrO_xF_y contains disordered chromium species.

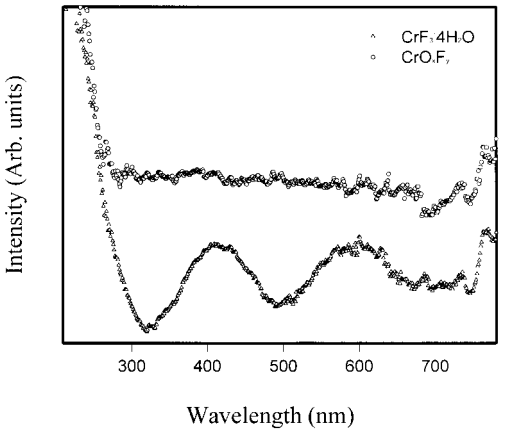

FIG. 4. PAS spectra for $CrF_3 \cdot 4H_2O$ (△) and CrO_xF_y (○).

A conductivity measurement has been done to investigate the electrical conductivity of CrO_xF_y. CrO_xF_y shows a significant conductivity, which is consistent with the fact that this sample does not show a charging effect in XPS measurements. The activation energy E_a, obtained from the plot of ln(conductivity) versus $10^3/T$, (K^{-1}) (not shown here), is ca 0.19 eV. Here, E_a is equal to $E_g/2$ (half the band gap energy) for an intrinsic semiconductor. On the other hand, in highly disordered solids such as amorphous semiconductors, E_a corresponds to the energy necessary to overcome the potential well of localized states and to hop to a neighboring site (25). For the CrO_xF_y case, the latter assignment of E_a seems to be more suited since CrO_xF_y contains phases with a high degree of lattice disorder.

We have measured the XPS valence band spectra (Fig. 5) for the two samples to monitor directly the changes of the density-of-states (DOS) in the valence band region affected by the lattice disorder. The peak at ~9 eV in $CrF_3 \cdot 4H_2O$ is ascribed to F 2p, while the peak at ~4.7 eV is assigned to the Cr d-band. The energy gap (~2.6 eV) between the Fermi level and the valence band edge indicates that the $CrF_3 \cdot 4H_2O$ sample is an insulating material. Air-calcination of $CrF_3 \cdot 4H_2O$ (dotted line) gives rise to a dramatic change of the valence band structure. The valence band spectrum becomes broader and featureless compared to that of $CrF_3 \cdot 4H_2O$. In addition, the spectrum shows an increased DOS near the Fermi energy level. This valence band feature of the CrO_xF_y sample can be explained by the Anderson localization model (26). According to this model, the disordered arrays of atoms are presumed to have a disordered potential field, so that the energies of atomic orbitals vary randomly from site to site. Atoms with near-average energies are very likely to have some neighbors at similar energy and can form delocalized orbitals by their overlap. Atoms at exceptionally high or low energies, however, are unlikely to have similar neighbors, and so their orbitals may remain as isolated or localized states. This Anderson model suggests that the band of energy levels created from disordered solids may have two types of orbitals: those in the middle of the band extend through the solid as in a periodic lattice, and those close to the top and bottom of the band are localized in the vicinity of a particular atom. As a result, the region of localized states in the band will depend on the degree of disorder. Likewise, the lattice disorder of CrO_xF_y is believed to build up a nonperiodic potential, which results in the broadness of the Cr d-bands and an increase in the DOS near the Fermi level. In other words, DOS features between 3.2 and 0 eV in CrO_xF_y can be interpreted as localized states caused by the lattice disorder of CrO_xF_y. A similar example, in which the ion beam was shown to create localized, defect states in the silica bands and to increase the DOS near E_F has been reported (27). Then, the electrical conduction in the CrO_xF_y may be generated via a carrier hopping between these localized states as observed in amorphous semiconductors (25).

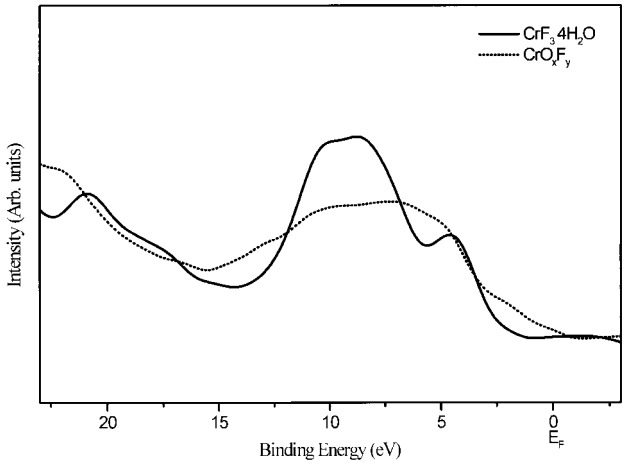

FIG. 5. XPS valence band spectra of $CrF_3 \cdot 4H_2O$ and CrO_xF_y.

To elucidate the relationship between the increased localized states and the catalytic activity in our chromium catalysts, first of all, we need to understand how the chromium species catalyze a fluorination reaction. Kijowski *et al.* (28) proposed a fluorination mechanism at the fluorinated chromia surface. According to their mechanism, the key to the catalytic reaction is the existence of labile fluorine which is weakly coordinated to the Lewis acidic chromium. This labile fluorine is produced as follows:

$$\text{HF (weakly adsorbed)} \leftrightarrow \text{catalytically active F} \rightarrow \text{Cr}^{\text{III}}\text{–F}.$$

Vacant sites for the coordination of labile fluorine exist in the coordinatively unsaturated chromium species on the surface. This argument can be applied to our system because of a similarity of the catalyst surface.

We suppose that the labile fluorine is formed initially by the chemisorption of a HF molecule and subsequent breaking of the H–F bond on the surface. The bond breaking can be initiated by electron transfer from the catalyst

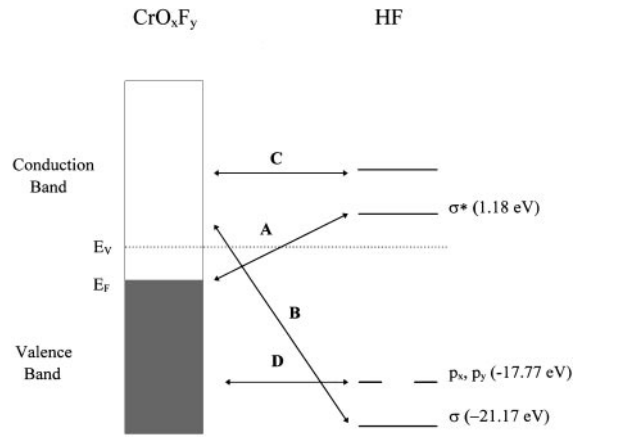

FIG. 6. The orbital–band interaction diagram. A (B) represent the attractive interaction between the valence (conduction) band of CrO_xF_y and the unoccupied (occupied) orbitals of HF. C (D) represent the repulsive interaction between the valence (conduction) band and the occupied (unoccupied) orbitals. E_v and E_F denote the vacuum level and Fermi energy level, respectively.

surface to the HF molecule or vice versa, which results in a reduction of the bond order in the HF molecule. The CrO_xF_y catalyst, which has more localized states, is more likely to interact more effectively with HF than $CrF_3 \cdot 4H_2O$, because of its higher DOS at the Fermi level as observed in Fig. 5. This situation can be explained by the orbital–band interaction diagram in Fig. 6. Direct interactions between CF_3CH_2Cl molecules and the catalyst surface are not considered because adsorption strength of CF_3CH_2Cl molecules was known to be about 150 times smaller than that of HF molecules (29). Here, the orbital energies of the HF molecule are calculated by the HF/6-311++g** method with a Gaussian 94 package (30). A chemical interaction can be analyzed from the starting point of energy levels of the interacting partners. According to second-order perturbation theory (31), the interactions between the two systems are pairwise additive over molecular orbitals and each pair interaction is governed by

$$\Delta E = \frac{H_{ij}^2}{E_i - E_j},$$

where ΔE indicates the strength of the interaction between orbital i and j of the interacting partners. E_i and E_j represent the orbital energies of ith and jth levels, respectively. H_{ij} corresponds to the matrix element of the perturbation Hamiltonian between state i and j. This concept is usefully adopted for the interaction of a molecule with the solid surface (32). Here, as shown in Figs. 6, A and B represent the attractive interactions, and C and D, the repulsive interactions. The A-type interaction denotes the interaction between the valence band of the catalyst surface and the antibonding orbitals of the HF molecule, and the B-type interaction between the conduction band of the catalyst surface and the bonding orbitals of the HF molecule. According to this diagram, the CrO_xF_y catalysts which have a higher DOS around the E_F level than $CrF_3 \cdot 4H_2O$ will show a stronger attractive interaction of A- and B-types with HF molecules than $CrF_3 \cdot 4H_2O$. As a result, the HF molecules are likely to adsorb more strongly on the CrO_xF_y surface than on $CrF_3 \cdot 4H_2O$. We can explain the enhanced catalytic activity as follows. The adsorbed HF molecules decompose on the CrO_xF_y surface and then generate labile fluorine on the surface. The fluorinated surface is now catalytically active for the fluorination reactions.

To our best knowledge, this is the first report to use PAS, conductivity measurements, and valence band results in the characterization of the fluorination catalyst, suggesting the importance of the electronic property in the fluorination catalytic activity. This argument is expected to be applied to the other fluorination catalysts, e.g. Cr_2O_3 (33), which show a valence band feature similar to that of our CrO_xF_y catalyst.

IV. CONCLUSION

The XRD pattern of air-calcined product of $CrF_3 \cdot 4H_2O$ indicates that the resulting material contains a predominantly noncrystalline phase. The XPS and PAS measurements also show that the air-calcined product consists of various chromium compound phases. The valence band spectra of the air-calcined product show an increased DOS near the Fermi energy level relative to the $CrF_3 \cdot 4H_2O$ phase. The increased DOS can be explained by the Anderson localization model. The higher catalytic activity of the air-calcined product CrO_xF_y relative to $CrF_3 \cdot 4H_2O$ is likely due to the stronger attraction between the catalyst surface with more localized states and the HF molecules.

ACKNOWLEDGMENTS

The authors thank Dr. C. Hwang for XPS measurements and M. H. Ryoo and S. E. Lee for PAS measurements. This work was supported in part by the Center of Molecular Science and the Korea Institute of Science and Technology.

REFERENCES

1. Webb, G., and Wenfield, J., *Chem. Br.* **28**, 996 (1992).
2. Nelson, T. P., and Wevill, S. L., *in* "Alternative Formulations and Packaging to Reduced Use of Chlorofluorocarbons." Noyes Data Co., New Jersey, 1990.
3. Manzer, L. E., *Catal. Today* **13**, 13 (1997).
4. Coulson, D. R., Wijnen, P. W. J. G., Lerou, J. J., and Manzer, L. E., *J. Catal.* **140**, 103 (1995).
5. U.S. Patent 4,792,643.
6. Japan patent application 6-65117.
7. European patent application 0554165Al.
8. Lee, B. G., Kim, H. S., Kim, H., Lee, S. D., and Seo, I., *J. Ind. & Eng. Chem.* **3**, 160 (1997).

9. Brunet, S., Requieme, B., Matouba, E., Barrault, J., and Blanchard, M., *J. Catal.* **152**, 70 (1995).
10. Ballinger, T. H., and Yates, J. T., *J. Phys. Chem.* **96**, 1417 (1995).
11. Ballinger, T. H., Smith, R. S., Colson, S. D., and Yates, J. T., *Langmuir* **8**, 2473 (1992).
12. Thomson, J., Webb, G., and Winfield, J. M., *J. Chem. Soc. Chem. Commun.*, 323 (1991).
13. Thomson, J., Webb, G., Winfield, J. M., Bonniface, D., Shortman, C., and Winterton, N., *Appl. Catal. Ser. A* **97**, 67 (1993).
14. Kemnitz, E., Kohne, A., Grohmann, I., Lippitz, A., and Unger, W. E. S., *J. Catal.* **159**, 270 (1996).
15. Kim, H., Kim, H. S., Lee, B. G., Lee, H., and Kim, S., *J. Chem. Soc., Chem. Commun.*, 2383 (1995).
16. Lee, H. J., Jeong, H. D., Chung, Y. S., Kim, H. S., Kim, S., and Chung, M. J., *J. Catal.* **169**, 307 (1997).
17. Merryfield, R., McDaniel, M., and Parks, G., *J. Catal.* **77**, 348 (1982).
18. Shuttleworth, D., *J. Phys. Chem.* **84**, 1629 (1980).
19. Carver, J. C., Schweitzer, G. K., and Carlson, T. A., *J. Chem. Phys.* **57**, 973 (1972).
20. Barrault, J., Brunet, B., Requieme, B., and Blanchard, M., *J. Chem. Soc., Chem. Commun.*, 374 (1993).
21. Niedersen, K.-U., Shreier, E., and Kemnitz, E., *J. Catal.* **167**, 210 (1997).
22. Brunet, S., Requieme, B., Motouba, E., Barrault, J., and Blanchard, M., *J. Catal.* **152**, 70 (1995).
23. Holmes, O. G., and McClure, D. S., *J. Chem. Phys.* **26**, 1686 (1957).
24. Huheey, J. E., *in* "Inorganic Chemistry," p. 384. Harper International Si edition, Harper, New York, 1983.
25. Hummel, R. E., *in* "Electronic Properties of Materials," p. 170. International Student Edition, Springer-Verlag, New York/Berlin, 1994.
26. Cox, P. A., *in* "The Electronic Structure and Chemistry of Solids," p. 221. Oxford Science, Oxford, 1986.
27. Barr, T. L., *in* "Modern ESCA," p. 152. CRC Press, Boca Raton, FL, 1994.
28. Kijowski, J., Webb, G., and Winfield, J. M., *Appl. Catal.* **27**, 181 (1986).
29. Kim, H., unpublished results.
30. Frisch, M. J., Trucks, G. W., Schlegel, H. B., Gill, P. M. W., Johnson, B. G., Robb, M. A., Cheeseman, J. R., Keith, T., Petersson, G. A., Montgometry, J. A., Raghavachari, K., Al-Laham, M. A., Zakrezewski, V. G., Ortiz, J. V., Foresman, J. B., Cioslowski, J., Stefanov, B. B., Nanayakkara, A., Challacombe, M., Peng, C. Y., Ayala, P. Y., Chen, W., Wong, M. W., Andres, J. L., Replogle, E. S., Gomperts, R., Martin, R. L., Fox, D. J., Binkley, J. S., Defrees, D. J., Baker, J., Stewart, J. P., Head-Gorden, M., Gonzalez, C., and Pople, J. A., "Gaussian 94, Revision D.2." Gaussian, Pittsburgh, PA, 1995.
31. Albright, T. A., Burdett, J. K., and Whangbo, M. H., "Orbital Interaction in Chemistry." Wiley, New York, 1985.
32. Hoffman, R., *in* "Solids and Surfaces: A Chemist's View of Bonding in Extended Structures," p. 108. VCH, Weinhein/New York, 1988.
33. Schrott, A. G., Frankel, G. S., Davenport, A. J., Isaacs, H. S., Jahnes, C. V., and Russak, M. A., *Surf. Sci.* **250**, 139 (1991).